ACCEPTED VERSION

Xianwen Hu, Ching Tai Ng, Andrei Kotousov

Scattering characteristics of quasi-Scholte waves at blind holes in metallic plates with one side exposed to water

Final publication at: http://dx.doi.org/10.1016/j.ndteint.2020.102379

http://hdl.handle.net/2440/129778

Journal article:

Xianwen Hu, Ching Tai Ng, Andrei Kotousov. (2021). Scattering characteristics of quasi-Scholte waves at blind holes in metallic plates with one side exposed to water. NDT & E International, 117:102379.

Scattering characteristics of quasi-Scholte waves at blind holes in metallic plates with one side exposed to water

Xianwen Hu[a], Ching-Tai Ng[a,*], Andrei Kotousov[b]

[a] School of Civil, Environmental & Mining Engineering, The University of Adelaide, SA 5005, Australia

[b] School of Mechanical Engineering, The University of Adelaide, SA 5005, Australia

Abstract

Corrosion is one of the major issues in metallic structures, especially those operating in humid environments and submerged in water. It is important to detect corrosion at its early stage to prevent further deterioration and catastrophic failures of the structures. Guided wave-based damage detection technique is one of the promising techniques for detecting and characterizing damage in structures. In water-immersed plate structures, most of the guided wave modes have strong attenuation due to energy leakage into the surrounding liquid. However, there is an interface wave mode known as quasi-Scholte waves, which can propagate with low attenuation. Therefore, this mode is promising for structural health monitoring (SHM) applications. This paper presents an analysis of the capability of quasi-Scholte waves in detecting internal corrosion-like defects in water-immersed structures. A three-dimensional (3D) finite element (FE) model is developed to simulate quasi-Scholte wave propagation and wave scattering phenomena on a steel plate with one side exposed to water. The accuracy of the model is validated through experimental measurements. There is good agreement between the FE simulations and experimental measurements. The experimentally verified 3D FE model is then employed in a series of parametric studies to analyze the scattering characteristics of quasi-Scholte waves at circular blind holes with different diameters and depths, which are the simplest representation of progressive corrosion. The findings of this study can enhance the understanding of quasi-Scholte waves scattering at corrosion damage of structures submerged in water and help improve the performance of in-situ damage detection techniques.

---

[*] Corresponding Author E-mail address: alex.ng@adelaide.edu.au

1. Introduction

Structures that have one side exposed to water are commonly encountered, such as water tanks, pipelines, and ship hulls. These structures often incorporate plate-like components, which are prone to corrosion as a result of electrochemical reactions in the presence of water. Corrosion can occur in a localized region and deteriorate the strength of the structures. It is important to detect and control corrosion so that catastrophic failures and leakage can be avoided.

Among various structural health monitoring (SHM) techniques [1-3], guided wave-based techniques have attracted increasing interest due to the ability to inspect large areas compared to the conventional non-destructive evaluation (NDE) techniques, high sensitivity to different types and small damage, and the ability to inspect inaccessible locations. A review of guided wave-based SHM techniques can be found in [4]. However, the majority of the studies on guided waves have focused on the structures with traction free boundary conditions [5-8]. Meanwhile, there are limited studies on using guided waves for safety inspections on structures submerged in water, especially the quasi-Scholte waves.

1.1. Damage detection of submerged structures using guided waves

Energy of guided waves in structures immersed in water can leak into the surrounding medium so that most of the guided wave modes have high attenuation characteristics, which significantly reduces the inspection area. As a result, the practical applications are limited to specific guided wave modes and the excitation frequencies need to be at their corresponding low attenuation frequency bands [9]. Several studies demonstrated the feasibility of using guided waves for the damage inspection in submerged structures. Na and Kundu [10] investigated the capability of the flexural cylindrical guided wave modes in detecting defects in underwater pipes. They found that the amplitudes of the transmitted signals would be decreased after they passed through various types of damage in pipes. This phenomenon could be used to evaluate the extent and distinguish the type of damage. Chen et al. [11] employed the fundamental antisymmetric leaky lamb wave mode (leaky A_0 waves) to evaluate corrosion damage in a submerged metallic plate. The amplitudes and the speed of leaky A_0 waves were found to be significantly affected by the surrounding fluid medium. Pistone et al. [12] used a pulsed laser to generate guided waves in a water-immersed aluminum plate and collected the wave signal by an array of immersed transducers. They concluded that the fundamental symmetric leaky lamb wave mode (leaky S_0 waves), which had the fastest wave speed and the

least decay, could be used to detect cracks and holes in the plate. Sharma and Mukherjee [13] used a pair of immersed ultrasonic transducers to generate and measure guided waves in a steel plate, both sides of which were fully immersed in water. Leaky S_0 waves, the first order symmetric leaky lamb wave mode (leaky S_1 waves), and the first order anti-symmetric leaky lamb wave mode (leaky A_1 waves) were excited at their corresponding low attenuation frequency bands. Each of these wave modes demonstrated a different sensitivity to notch-like defects and the decrease in amplitudes of the transmitted signal could be related to the severity of the damage. Takiy et al. [9] implemented experiment studies to verify the existence of guided wave modes at their theoretically predicted low attenuation frequency bands. It was confirmed that the higher order guided wave modes at their corresponding low attenuation frequency bands were also suitable to be used for damage detection in submerged structures.

1.2. Quasi-Scholte waves in immersed structure

In addition to the symmetric and anti-symmetric guided wave modes, there is an interface wave mode known as quasi-Scholte waves existing at the water-plate interface. This interface wave mode has low attenuation but it is rarely used for evaluating damage in structures since it has been reported that a large proportion of energy is propagating into the fluid at high frequencies [14]. However, it is found that most of the wave energy of the quasi-Scholte mode at low excitation frequencies is conserved in the structures during the propagation. Tian and Yu [15, 16] experimentally investigated guided wave propagation on a steel plate loaded with water on a single side. They used a scanning laser Doppler vibrometer to measure the wave signals along a line and plotted the data in the frequency-wavenumber spectrum. It was demonstrated that leaky A_0 waves were indiscernible at low frequencies due to high attenuation while quasi-Scholte waves appeared clearly. Recently, Hayashi and Fujishima [17] studied the feasibility of using quasi-Scholte waves for damage detection in a thin aluminum plate that had one side immersed in water. The scattered waves due to a through-thickness notch could be observed at the low-frequency range. It should be noted that this study only measured the reflected signals. The scattering characteristics were not investigated.

The practical application of the guided waves relies on a distributed transducer network, by which the guided wave signal is sequentially emitted by one of the transducers, and the rest of the transducers are used to measure the impinging waves. The majority of guided wave-based damage detection techniques employ the waves scattered at the damage and received by

the transducers at different directions to detect and identify the damage [5, 18-20]. Therefore, understanding the scattering characteristics at different directions plays an important role in the development of the guided wave-based damage detection techniques. In the literature, different studies investigated the scattering characteristics of guided waves at different types of defects. However, the majority of the studies focused on traction free conditions, and the scattering characteristics of guided waves in plates loaded with water have not been well investigated. In particular, there are very limited studies investigating the scattering characteristics of the interface wave mode, quasi-Scholte waves, in plates loaded with water.

This paper presents a comprehensive numerical and experimental analysis of the scattering characteristics of quasi-Scholte waves at corrosion-like defects in structures exposed to water, such as water tanks and pipelines. The numerical method using a three-dimensional (3D) finite element (FE) model is employed to investigate the guided wave propagation and scattering phenomena on a one-side water-immersed steel plate with a circular blind hole that represents a corrosion spot or wall thinning, which is exposed to water. The scattering characteristics are investigated in terms of scattering directivity patterns (SDPs), which display the energy distribution of the scattered waves around the damage. The findings of this study provide a guide on the selection of appropriated excitation frequencies and sensor locations to evaluate corrosion damage, which can advance the guided wave-based damage detection techniques for submerged structures.

This paper first presents the theoretical predication of guided waves traveling along a steel plate that has one side submerged in water in Section 2. Sections 3 and 4 describe the 3D FE simulation and experimental verification, respectively. The accuracy of the simulation results is validated through experimental measurements. Then, a series of numerical studies are carried out using the experimentally verified 3D FE model to investigate the characteristics of the scattered quasi-Scholte waves at blind holes with different dimensions in Section 5. Finally, discussion and conclusion are provided and drawn in Sections 6 and 7, respectively.

2. Guided waves in one-side water-immersed plates

Guided waves in plate-like structures are comprised of multiple symmetric and anti-symmetric wave modes, which are represented by symbols S_i and A_i, respectively, with the subscript ($i = 0,1,…$) representing the order of the wave modes. The majority of the studies consider the plates that are placed open to the air. The boundary conditions for the top and bottom sides of

the plates are traction-free as shown in Fig. 1(a). The characteristic equation of the guided waves can be described as [21]
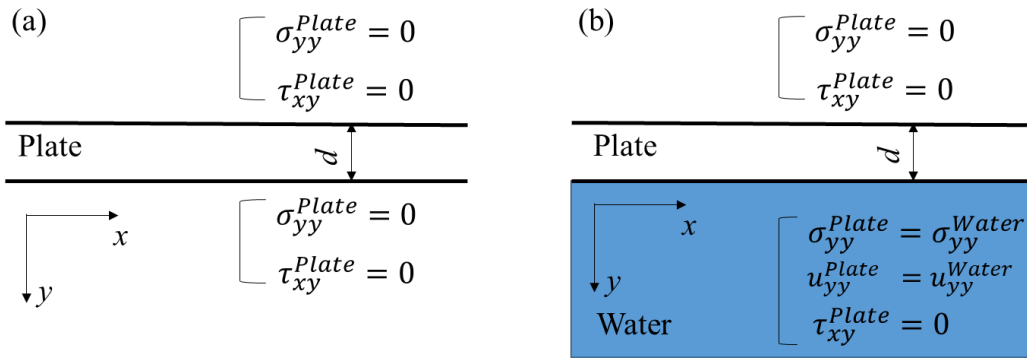
$$\frac{\tan(qh)}{\tan(ph)} = -\frac{4k^2 qp}{\left(k^2 - q^2\right)^2} \tag{1}$$

for symmetric modes S_i, and

$$\frac{\tan(qh)}{\tan(ph)} = -\frac{\left(k^2 - q^2\right)^2}{4k^2 qp} \tag{2}$$

for anti-symmetric modes A_i, where $h = \dfrac{d}{2}$; $q^2 = \dfrac{w^2}{c_T^2} - k^2$; $p^2 = \dfrac{w^2}{c_L^2} - k^2$; d, w, and k represent the plate thickness, circular frequency and wavenumber, respectively; c_L and c_T are the longitudinal wave speed and the transverse wave speed of the plate, respectively. It can be seen from Equations (1) and (2) that the characteristics of guided wave modes depend on the product of the plate thickness and the frequency. The solutions can be presented as guided wave dispersion curves that describe the relationship between the frequency-thickness product and the characteristics of the guided wave modes.

(a)
$$\begin{bmatrix} \sigma_{yy}^{Plate} = 0 \\ \tau_{xy}^{Plate} = 0 \end{bmatrix}$$

Plate

d

x

$$\begin{bmatrix} \sigma_{yy}^{Plate} = 0 \\ \tau_{xy}^{Plate} = 0 \end{bmatrix}$$

y

(b)
$$\begin{bmatrix} \sigma_{yy}^{Plate} = 0 \\ \tau_{xy}^{Plate} = 0 \end{bmatrix}$$

Plate

d

x

$$\begin{bmatrix} \sigma_{yy}^{Plate} = \sigma_{yy}^{Water} \\ u_{yy}^{Plate} = u_{yy}^{Water} \\ \tau_{xy}^{Plate} = 0 \end{bmatrix}$$

y

Water

Fig. 1. Boundary conditions (a) free plate; and (b) one-side water-immersed plate

When one side of the plate is immersed in water, as shown in Fig. 1(b), the interface between the water and the plate is no longer traction free and the guided wave propagation changes [22]. The wave energy can leak into the water through out-of-plane motions of the particles at the water-plate interface. However, the displacements of the water and the plate are

discontinuous in the shear direction because water cannot sustain shear loads [23, 24]. The governing equations of guided waves in the one-side water-immersed plate can be expressed as [25, 26]

$$\det\left(G\left(w,k,c_w,c_T,c_L,d,\rho_w,\rho\right)\right)=0 \qquad (3)$$

where c_w and ρ_w represent the bulk wave speed and density of water, respectively. G represents the characteristic matrix for the coupled fluid and solid waveguide. By solving Equation (3), one can obtain the dispersion curves of guided waves for the one-side water-immersed steel plate.

The calculation can be done by the commercial software DISPERSE, which employs the global matrix method to calculate dispersion curves in a multi-layer waveguide [27]. In this method, the bulk wave characteristics of each layer are first determined from the corresponding material properties. Then, the stresses and displacements in each layer can be expressed in terms of the partial waves, which are assembled into one large global matrix with the boundary conditions. The global matrix can be solved for its modal response to find valid combinations of a certain frequency, wavenumber, and attenuation. The process repeats until all dispersion curves are traced.

Fig. 2 shows the phase velocity and attenuation dispersion curves of a steel plate that has its bottom surface immersed in water. There are three wave modes within the frequency-thickness band up to 1MHz-mm: quasi-Scholte waves, leaky A_0 waves, and leaky S_0 waves. Unlike leaky A_0 waves and leaky S_0 waves, quasi-Scholte waves are one of the interface wave modes that have most energy concentrated at the water-plate interface instead of radiating into the liquid [28]. In general, the phase velocity of quasi-Scholte waves, at given excitation frequency, is much smaller than leaky S_0 waves and leaky A_0 waves as shown in Fig. 2(a). Smaller phase velocity means a shorter wavelength, which means higher sensitivity to small defects [11]. In addition, the attenuation of quasi-Scholte waves is almost zero for the entire frequency-thickness range (Fig. 2(b)). Therefore, quasi-Scholte waves theoretically have the potential for long-range inspection, and are expected to have a high sensitivity to damage.
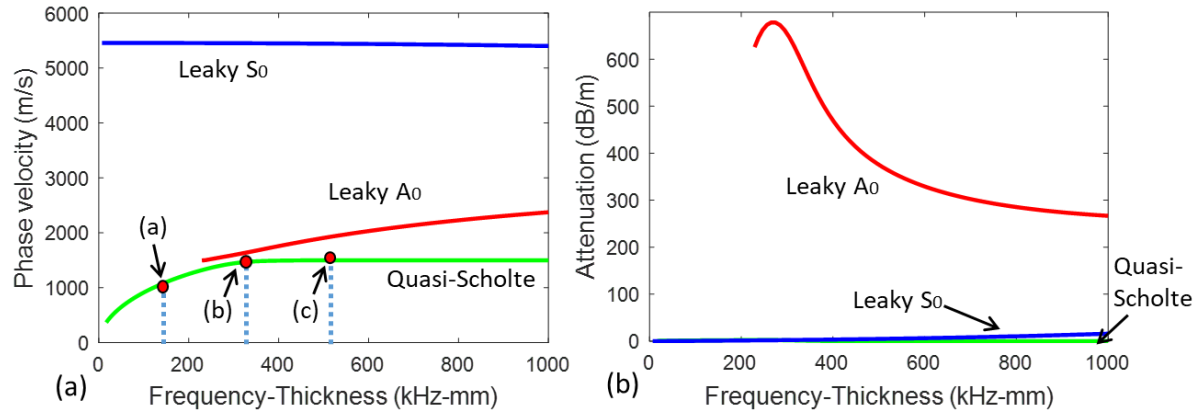
Fig. 2. (a) Phase velocity and (b) attenuation dispersion curves of 1 mm thick steel plate with one side immersed in water

Figs. 3(a)-(c) present the mode shapes of quasi-Scholte waves at 100kHz-mm, 300kHz-mm, and 500kHz-mm as denoted by the three red dots in Fig. 2(a). It should be noted that the mode shape diagram only demonstrates the maximum amplitudes of the in-plane displacements and the out-of-plane displacements. A 1mm thick steel plate is located in the upper region while the bottom region represents the half-space water area. It can be seen that the displacements in the plate comprise the main part of the total displacements at the frequency-thickness range lower than 300kHz-mm. This range is known as the dispersive region, in which the phase velocity of quasi-Scholte waves changes significantly with the product of the frequency and plate thickness as shown in Fig. 2(a). The range of frequency-thickness over 300kHz-mm is the non-dispersive region. In this region, the phase velocity of the quasi-Scholte wave is almost constant. However, the deformation of the modeshape in the plate is negligible compared to the deformation of the modeshape in the water as shown in Fig. 3(c). Due to this observation, the quasi-Scholte wave in the non-dispersive region cannot be detected from the dry plate surface since most of the wave energy concentrates at the waterside of the submerged plate. Therefore, the rest of the study focuses on the frequency-thickness product values lower than 300kHz-mm.
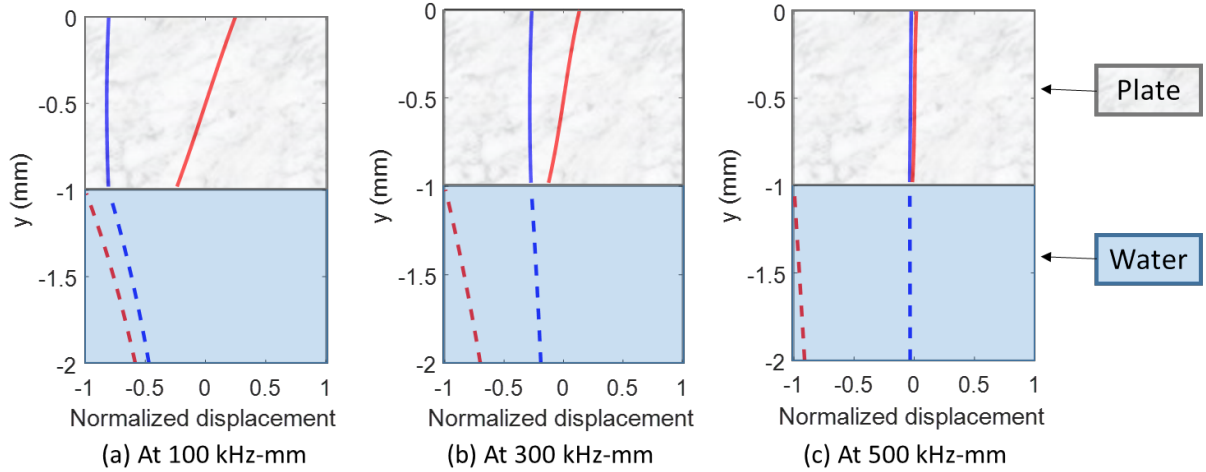
Fig. 3. Theoretical mode shapes of quasi-Scholte waves (red line denotes in-plane displacements; blue line denotes out-of-plane displacements)

3. Wave propagation and interaction simulation

3D FE simulation was used to simulate guided wave propagation on a steel plate loaded with water on a single side. The commercial FE software, ABAQUS, was used to generate the geometry and mesh the FE model. This study aims to investigate the interaction of quasi-Scholte waves with blind holes, which is a local phenomenon. Therefore, only a rectangular section of the plate was modeled with absorbing regions attached to its edges to reduce unwanted waves reflected from the boundaries and improve the computational efficiency. Fig. 4 shows the configuration of the 3D FE model. The dimension of the steel plate was 270mm×320mm×2mm ($W \times L \times H$) with 40mm wide absorbing regions applied to its edges. The bottom surface was in contact with a 100mm thick water layer. Table 1 summarizes the material properties of the steel plate and the water for the 3D FE model. The plate and absorbing regions were discretized by 3D eight-node reduced integration solid elements (C3D8R). The water layer was modeled using 3D eight-node reduced integration acoustic elements (AC3D8R). The interface between the water and the steel plate was defined by surface-based tie constraint in ABAQUS/Explicit, which tied the acoustic pressure on the fluid surface with the displacements on the solid surface [29]. This allowed the wave energy in the plate to transmit into the water through the out-of-plane displacements.

Table 1 Material properties of the steel and water used in the 3D FE model

	Density (kg/m^3)	Young's modulus (GPa)	Poisson's ratio	Bulk modulus (GPa)
Plate	7800	200	0.3	--
Water	1000	--	--	2.2
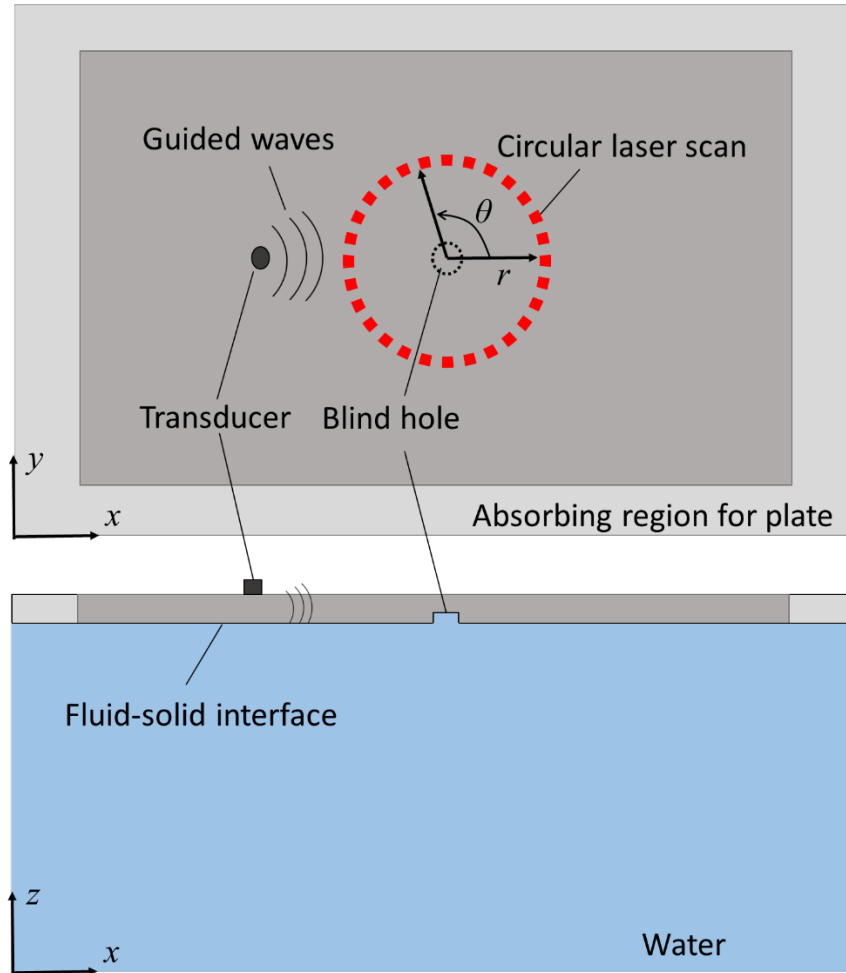
Fig. 4. Schematic diagram of the configuration used in FE simulation

The guided waves were excited on the top water-free surface through applying the out-of-plane nodal displacements by a 5mm diameter circular transducer [30, 31]. The excitation signal was a five-cycle Hann window-modulated sinusoidal tone bust [32]. In order to compare the FE simulations with experiment results, the excitation frequency in this study was selected as 100kHz, at which the measured signal in the experiment had the highest signal-to-noise ratio. At this excitation frequency, the theoretical wavelength of the selected wave mode, the quasi-Scholte wave, was around 10mm as predicted by the phase velocity dispersion curves. Then,

the in-plane dimension of the solid elements in the plate was set as $0.5 \times 0.5 \text{mm}^2$, which was small enough to ensure that at least ten elements exist per wavelength of the selected wave mode as recommended in the literature to simulate guided wave interaction with defects [33, 34]. Eight layers of solid elements were used in the thickness direction, by which the aspect ratio of the elements was two. A convergence study was implemented to confirm that the accuracy of the simulation results using elements with the aspect ratio of two was the same as that using the cubic elements.

The absorbing regions located at the four edges of the plate were divided into 40 layers of which the mass-proportional damping coefficients (C_M) gradually increased from the innermost layer to the outmost layer. The absorbing layers can avoid the wave reflections from the boundaries, and hence, it allows using a small FE model to analyze the wave propagation and the scattering phenomena in a large structure. The mass-proportional damping coefficient of each absorbing layer was defined as [35, 36]

$$C_M = C_{M\max}X(x^3) \tag{4}$$

where x represents the distance between the current layer and the interface between the absorbing regions and the steel plate; X denotes a function of x, whose value varies from 0 when $x = 0$ to 1 at the outmost layer of the absorbing region $x = x_{\max}$; $C_{M\max}$ is the mass-proportional damping coefficient of the outmost layer in the absorbing region and was set as 3×10^6, which was obtained by trial and error [37].

The dynamic simulations were accomplished by the explicit module of ABAQUS, which used the central-difference integration. For wave propagation problems, it is recommended that the time step increment should be less than the ratio of the minimum element size to the speed of the dilatational wave. In this study, the increment time step was automatically determined by ABAQUS in all simulations [38].

Figs. 5(a) and 5(b) present the snapshots of the simulated out-of-plane displacements in the 2mm-thick one-side water-immersed steel plate before and after the guided wave interaction with a circular blind hole, respectively. The excitation frequency was 100kHz and the corresponding frequency-thickness product was 200kHz-mm, which was in the dispersion region of quasi-Scholte waves. The diameter and depth of the blind hole were 10mm and 1.5mm, respectively. Guided waves were excited and propagated omnidirectionally and

gradually diminished when it reached the absorbing layers as shown in Fig. 5(b). There were no obvious boundary reflections observed from the plate edges. After the interaction of the incident waves with the circular blind hole, part of wave energy transmitted through and there were some waves reflected from the blind hole. Figs. 5(c) and 5(d) show the contour snapshot of the corresponding acoustic pressure in the water. It can be seen that there was only one wave packet observed in the plate. This wave packet had a flexure mode shape and most of the wave energy was confined to the water-plate interface rather than radiating into water. Due to these features, it was identified that this wave packet was related to the quasi-Scholte mode. The simulation results demonstrated that the out-of-plane excitation on the surface of the one-sided water-loaded plate dominantly generates the quasi-Scholte waves that are able to detect damage at the water-plate interface by wave scattering.
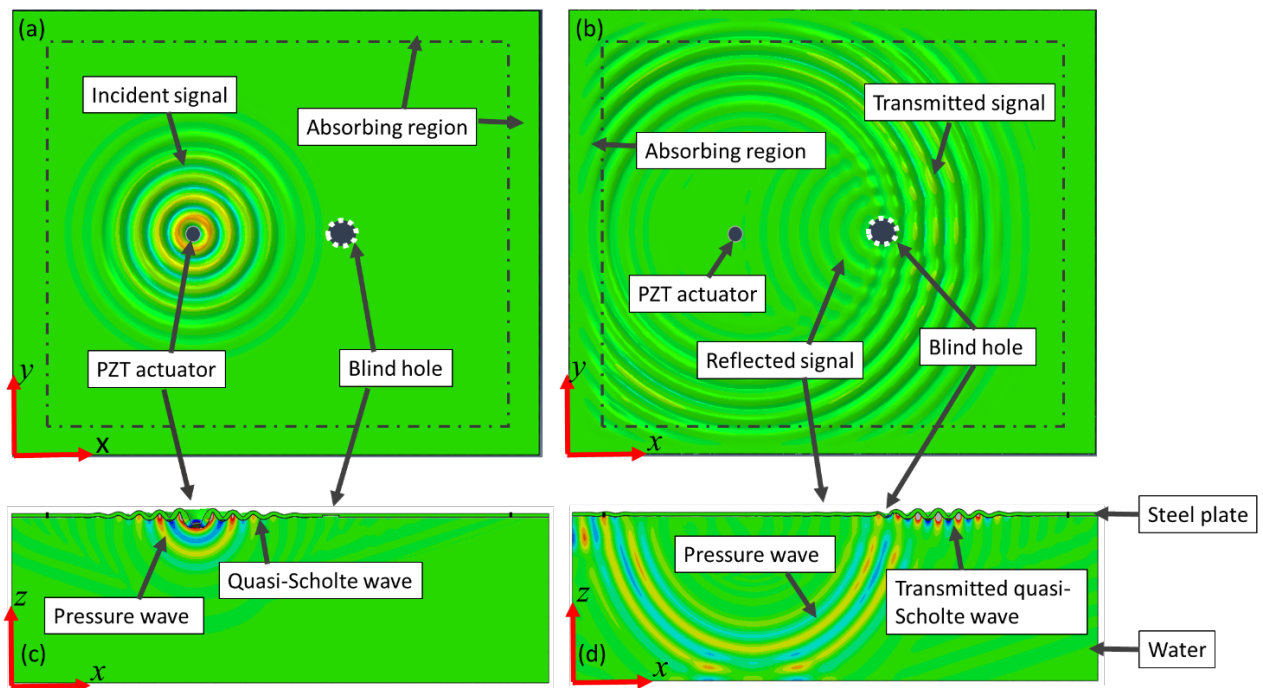
Fig. 5. Snapshots of the simulated out-of-plane displacements in a 2mm thick one-side water-immersed steel plate at different time instances; (a) before incident wave reach the circular blind hole; (b) after interaction of the incident wave with the circular blind hole; (c) and (d) the corresponding contour snapshots of the acoustic pressure.

4. Experimental validation

To study the wave propagation in a plate with one side exposed to water, a test metal tank was designed with the front wall being the test plate as shown in Fig. 6(a). The test plate was a 2mm thick steel plate and the material properties are given in Table 1. During the test, the metal tank was filled with water so that the internal surface of the test plate was in contact with water while the external surface of the test plate was exposed to the air. To validate the accuracy of the 3D FE model to simulate guided wave scattering phenomena, a blind hole was drilled at the internal surface of the test plate to model a corrosion pit (see, Fig. 6(b)). A Cartesian coordinate system was defined with the origin being located at the left bottom of the test plate (see, Fig. 6(a)). A circular piezoceramic transducer (5mm diameter, 2mm thickness) was mounted to the outer side (water-free surface) of the test plate at x=200mm and y=200mm, and it was used as the actuator to excite guided wave bursts. The excitation signal was generated by a function generator (AFG 3021B) and the voltage was increased by an amplifier (Krohn-Hite 7500). The out-of-plane displacements at various scanning points were measured by the non-contact laser scanning Doppler vibrometer (Polytec PSV-400-M2-20). The excitation signal was a five-cycle Hann window-modulated sinusoidal tone burst. The experimentally measured data were collected with a sampling rate of 10.26MHz. The measured signals were filtered by applying a band-pass filter and averaging procedure applied to 1000 recordings. The overall experiment setup is shown in Fig. 6(c).
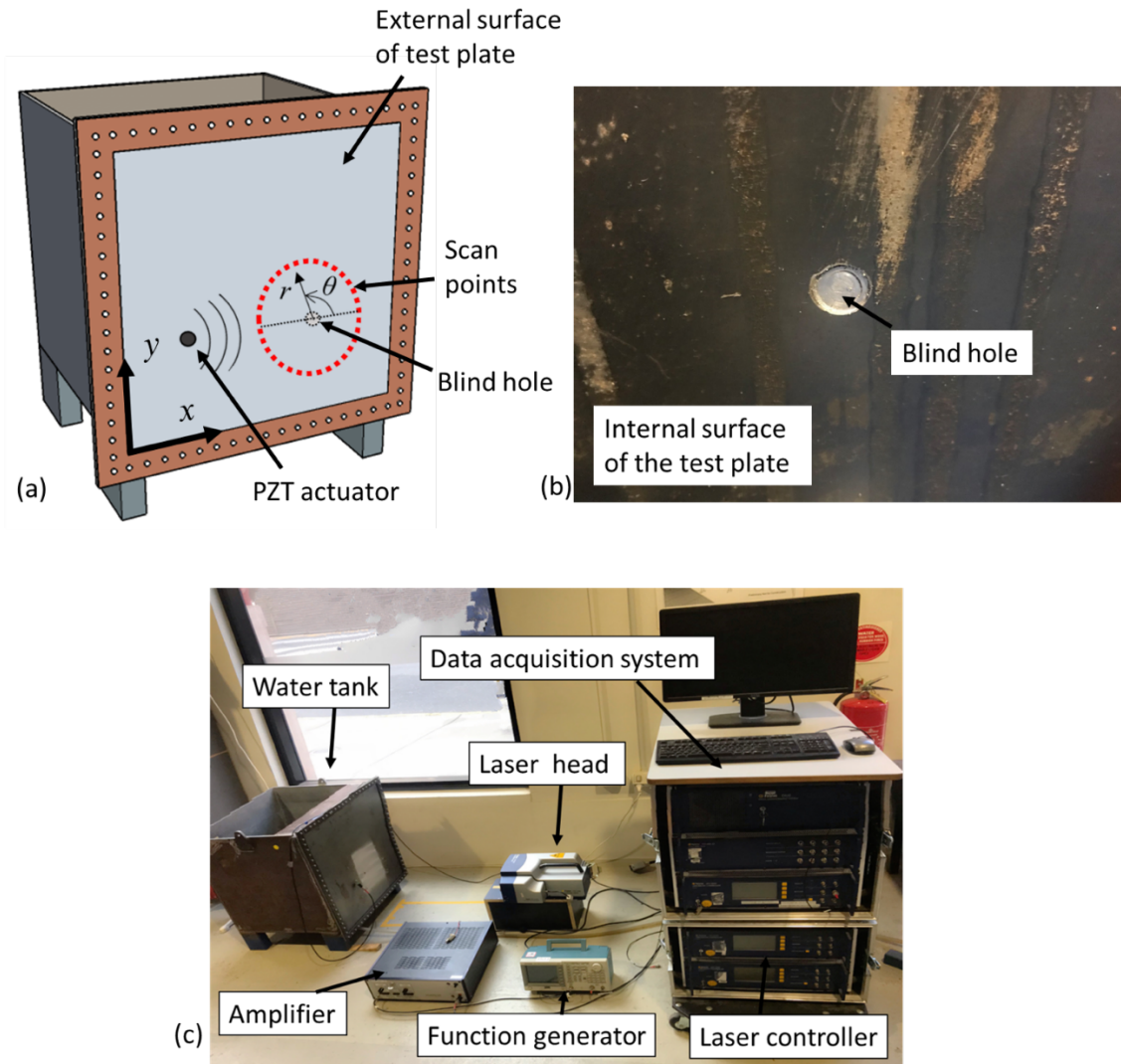
Fig. 6. (a) Schematic diagram of the water tank and; (b) blind hole at the internal surface of the test plate; and (c) the experiment setup

4.1. Verification of the intact FE model

This section details the outcomes of the experimental study on guided wave propagation in the intact steel plate (before drilling the blind hole) with one side exposed to water. Fig. 7(a) compares the FE simulated and experimentally measured signal in the time domain and the excitation frequency is 100kHz. There is good agreement between the FE simulations and experimental measurements. The results confirm that the signal measured at the water-free surface of the one-side water-immersed plate is dominated by a single wave packet, which is identified as quasi-Scholte mode as discussed in Section 3. At such excitation frequency, leaky S_0 waves have negligible out-of-plane components [15, 39] and the magnitudes of leaky A_0 waves are too small to be observed due to its high attenuation characteristics as shown in Fig.

2(b). To further investigate the accuracy of the 3D FE model, the phase velocity dispersion curves were calculated with the same strategy for the experimental measurements and FE simulations.

The excitation frequency was swept from 70kHz to 150kHz in steps of 10kHz. In this frequency range, the measured signals had a good signal-to-noise ratio in the experiment. At each excitation frequency, the out-of-plane displacements were collected at eleven points along the horizontal direction with a spatial step of 2mm, which was less than half of the wavelength of the quasi-Scholte wave mode. The measured time domain signals were then transformed into the frequency domain by fast Fourier transform (FFT). After that, the phase of each measured signal was calculated and the phase velocity between two measurements was calculated by

$$C_p = \frac{2\pi f \Delta\phi}{\Delta x} \tag{5}$$

where $\Delta\phi$ and Δx are the phase difference and distance between the two measurement points, respectively. C_p and f are the phase velocity and the central frequency of the excitation, respectively. The phase velocity at each excitation frequency was determined by taking the average of the calculated phase velocities at the measurement points. Fig. 7(b) presents the phase velocity dispersion curves of quasi-Scholte waves calculated by DISPERSE, FE simulations, and experimental measurements. The maximum deviation is less than 2%. There is good agreement between the theoretically calculated, numerically simulated, and experimentally measured phase velocity dispersion curves.

The measured signals were also converted into the time-frequency spectrum by short-time Fourier transform (STFT) to determine the traveling time of quasi-Scholte waves. The group velocity was calculated by

$$C_g(f_c) = \frac{\Delta x}{\Delta t} \tag{6}$$

where Δt is the difference of the time of arrival between the two measurement points, which were away from each other by Δx. For the excitation frequency of 100kHz, the group velocities obtained from the FE simulations and the experimental measurements are 2143 m/s and 2131 m/s, respectively. They are very close to the theoretical value of 2143 m/s calculated

by DISPERSE. Therefore, it can be concluded that the FE model can accurately simulate the wave on the steel plate loaded with water on a single side.
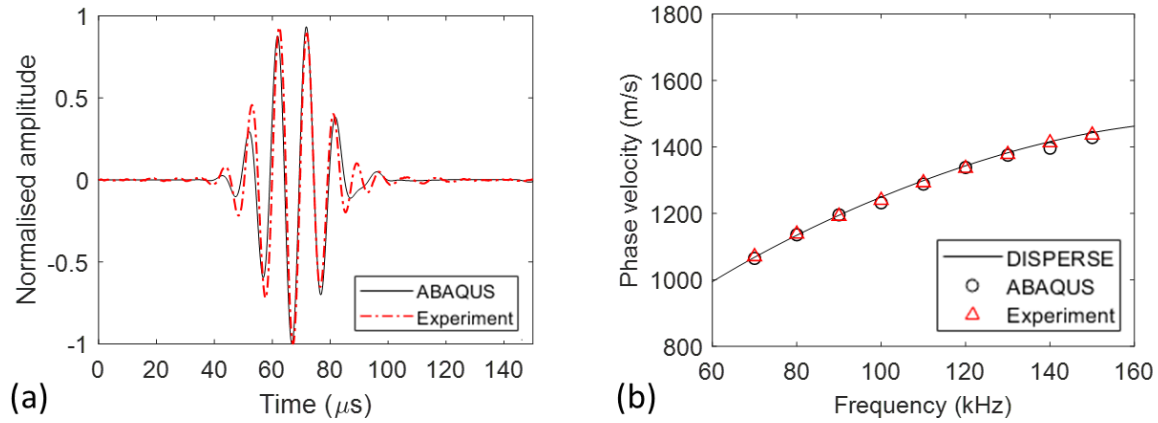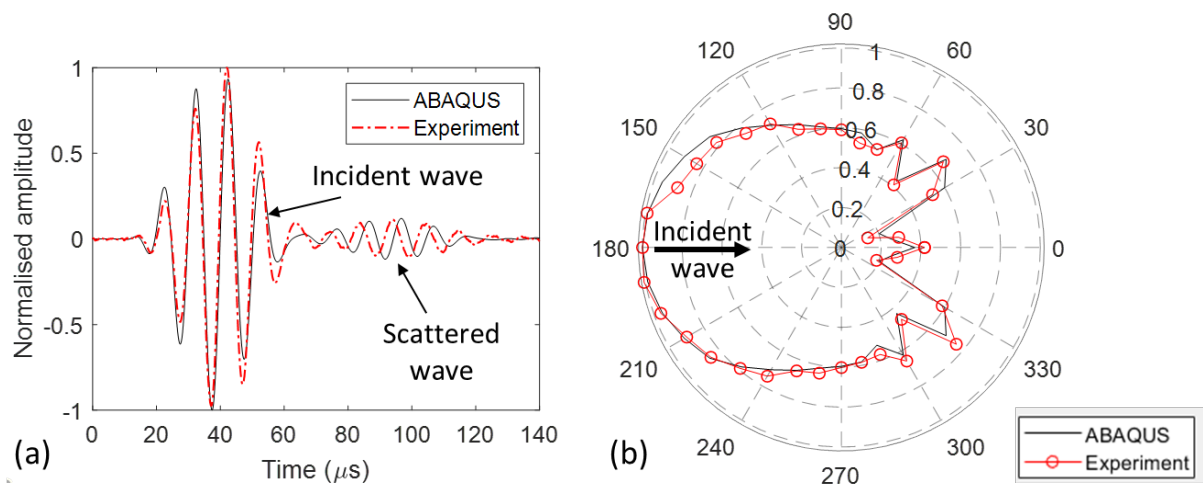

Fig. 7. (a) Typical FE simulated and experimentally measured signal at 100 kHz (black solid lines: simulation results; red dash lines: experimental results); (b) Phase velocity dispersion curves from the theoretical calculation (solid black line), FE simulations (black circles), and experimental measurements (red triangles).

4.2. Guided wave scattering at a blind hole

The accuracy of wave scattering simulation using the 3D FE model was investigated through experimental measurements. A circular blind hole was drilled at the internal surface of the plate as shown in Fig. 6(b). The depth and the diameter of the blind hole were measured to be 1.3mm and 12mm, respectively. A polar coordinate system was defined with the origin being the center of the blind hole as shown in Fig. 6(a). Incident waves were excited by a piezoceramic transducer located at $r = 80$mm and $\theta = 180°$. Scanning laser Doppler vibrometer was employed to scan a circular path covered by 36 points at $r = 50$mm, from $0°$ to $360°$ with the increment step of $10°$. The 3D FE model of the damaged plate with the same dimensions has a blind hole at the water-plate interface. The same strategy was employed to obtain the simulated out-of-plane displacements at the same 36 locations at the top surface (water-free surface).

Fig. 8(a) shows a typical signal obtained from the FE simulations and experimental measurements. The measurement point was located at $r = 50$mm and $\theta = 170°$. The incident wave was the selected interface wave mode, the quasi-Scholte wave, and a small magnitude of the scattered wave, which was generated by the interaction of the quasi-Scholte wave with the blind hole. There is a small phase shift in the scattered waves, which could be the result of a

small misalignment of the blind hole between the 3D FE model and the experiment. However, the simulated scattering amplitudes relative to the incident wave were consistent with the experimental measurements. Fig. 8(b) shows the maximum absolute amplitudes of the simulated and the experimentally measured signals, where the amplitudes were normalized by the peak amplitudes of the signal at r =50 mm and θ =180º. In general, the 3D FE model well predicted the experimental results. It should be noted that although this study focuses on a particular excitation frequency, the 3D FE model can simulate wave propagation for other excitation frequencies as long as the size of elements is small enough to meet the minimum number of the FE nodes per wavelength requirement.


Fig. 8. (a) FE simulated and experimentally measured signal at r=50mm, θ=170º of the one-side water-immersed steel plate with a blind hole; (b) Polar directivity patterns of the normalized maximum absolute amplitudes of quasi-Scholte waves measured on the circular path.

5. Scattering of quasi-Scholte waves due to circular blind holes at the water-plate interface

The experimentally validated 3D FE model was employed in a series of parametric studies to analyze the scattering characteristics of quasi-Scholte waves at circular blind holes at the water-plate interface. The simulations were carried out for the model with and without the blind hole so that the scattered waves could be extracted by subtracting the signals of the intact model from those measured from the model with the blind hole. The center of the blind hole was set as the origin of the polar coordinate system. Guided waves were generated on the water-free

side by a 5mm diameter circular transducer, of which the center was located at $r = 80$mm and $\theta = 180°$. The normal displacements were obtained at 36 nodal points which were located at $r = 50$mm and $0° < \theta < 360°$ with a $10°$ step increment. Then, the SDPs were determined by plotting the maximum magnitudes of the scattered waves in all directions around the blind hole. The amplitudes of the SDPs were normalized by the maximum absolute amplitudes of the wave signal at $r = 50$ mm and $\theta = 180°$. Figs. 9(a)-9(c) show the SDPs of the 100kHz incident quasi-Scholte waves at the 2, 6, and 10mm diameter circular blind holes with the depth of 0.5mm located at the water-plate interface. The results indicate that the SDPs are dependent on the size of the circular blind hole. For the 2mm diameter circular blind hole, the amplitudes of the reflected waves are comparable to the forward scattering amplitudes. However, the forward scattered waves increase significantly for the blind hole with larger diameters. The following sections investigate the effect of the diameter and the depth of the blind hole on the SDPs.
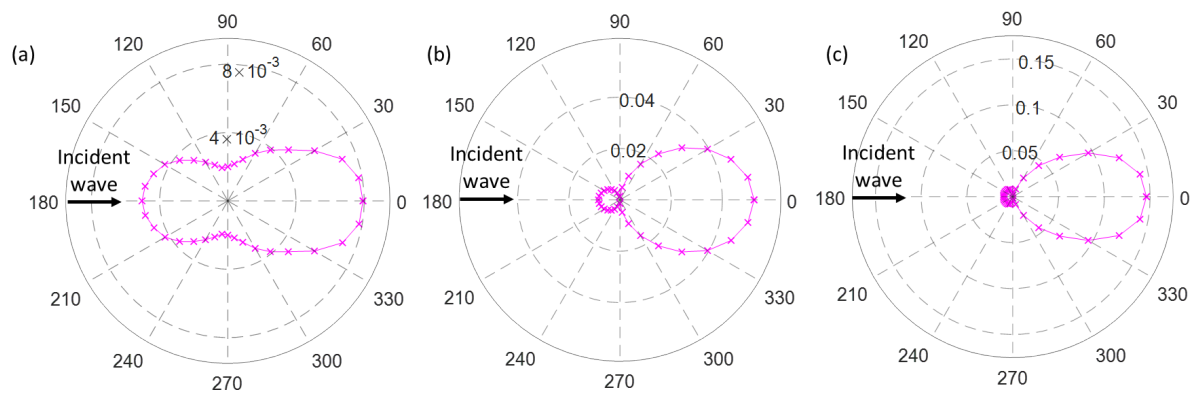

Fig. 9. SDPs for the one-side water-loaded plate with (a) 2mm, (b) 6mm, and (c) 10mm diameter circular blind hole with 0.5mm depth.

5.1. Influence of the diameter of the circular blind hole

The SDPs of quasi-Scholte waves have shown to change significantly with the size of the blind hole. This section explores the effect of the diameter of the blind hole on the scattering phenomenon in terms of the blind hole diameter to wavelength ratio (R_{DW}). For a circular blind hole with a depth of 0.5mm, the forward scattering amplitudes are given in Fig. 10(a) at $\theta = 0°$, $20°$, $40°$, $60°$, $80°$, $280°$, $300°$, $320°$, $340°$. For $\theta = 0°$, $20°$, and $340°$, the amplitudes increase with R_{DW} and have relatively larger amplitudes than the other directions. The scattering amplitudes at $\theta = 40°$ and $320°$ rise until the R_{DW} reaches 1.2 then reduce with R_{DW}. The

magnitudes of the scattered waves at $\theta = 60^\circ$, 80°, 280°, and 300° are small and exhibit slight fluctuation with R_{DW}.

Fig. 10(b) presents the backward scattering amplitudes at $\theta = 100^\circ$, 120°, 140°, 160°, 180° 200°, 220°, 240°, 260°. It can be seen that the overall behavior of the scattering magnitudes in the backward direction is much more complicated than that in the forward direction. For $\theta = 180^\circ$, 200°, 160°, 220°, 140°, 240°, and 120°, the amplitudes fluctuate following a sinusoidal pattern but the overall trend is a slow increase. The minima of the scattering amplitudes at $\theta = 220^\circ$ and 140° and $\theta = 240^\circ$ and 120° are obtained with R_{DW} of around 1.2, which are slightly behind the minima of scattered waves at $\theta = 180^\circ$, 200° and 160°. Additionally, the amplitudes at $\theta = 260^\circ$ and 100° are considerably small and show moderate variation with R_{DW}. In general, the amplitudes of the backward scattered waves are smaller than those in the forward directions. Besides, the scattering amplitudes are almost negligible in the directions perpendicular to the incident waves. Therefore, a sensor located at these directions is unlikely to detect any differences between damaged and undamaged plates.
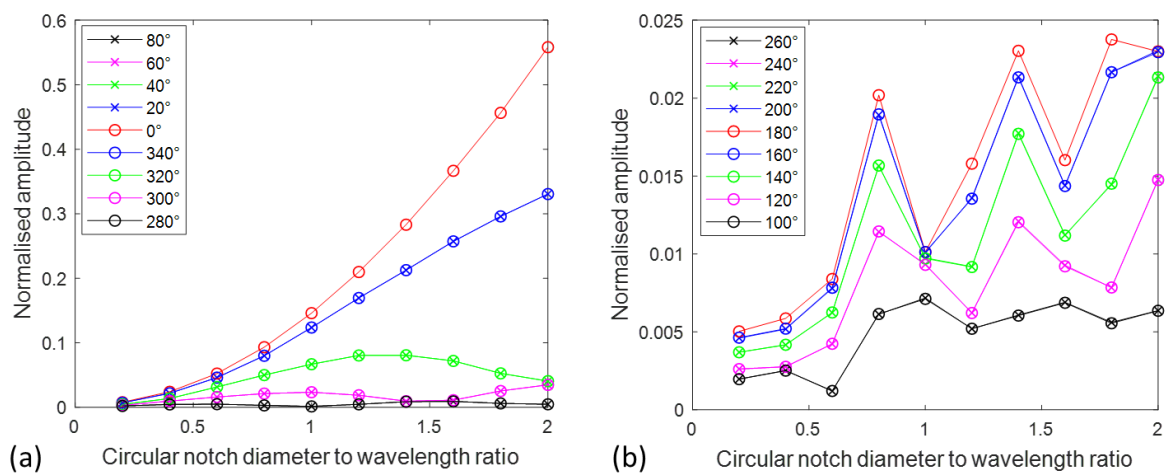
Fig. 10. Normalized amplitudes for (a) the forward scattered waves and (b) the backward scattered waves at a circular blind hole in the one-side water-loaded steel plate as a function of R_{DW}.

5.2. Influence of the depth of the circular blind hole

The above section demonstrates that the scattering characteristics are dependent on R_{DW}. This section shows that the SDPs of quasi-Scholte waves also relate to the depth of the circular blind hole. Figs. 11(a) and 11(b) show the SDPs of the 100kHz incident quasi-Scholte waves at the 6 mm diameter circular blind hole with the depth being 1.0 and 1.5mm located at the water-plate interface. Both the forward and backward scattering amplitudes increase with the depth of the blind hole. For shallow blind holes (Fig. 9(b) and Fig. 11(a)), the forward scattering amplitudes are much larger than the magnitudes of the backward scattered waves. However, the backward and forward scattering amplitudes are comparable in the case of deeper damage (Fig. 11(b)). In addition, the scattering amplitudes at the directions perpendicular to the incident wave are weak for shallow damage (Fig. 9(b) and Fig. 11(a)) but they become comparable to those at other directions for the deeper blind hole (Fig. 11(b)). Therefore, it can be seen that both the diameter and depth of the blind hole have a significant influence on the SDPs.
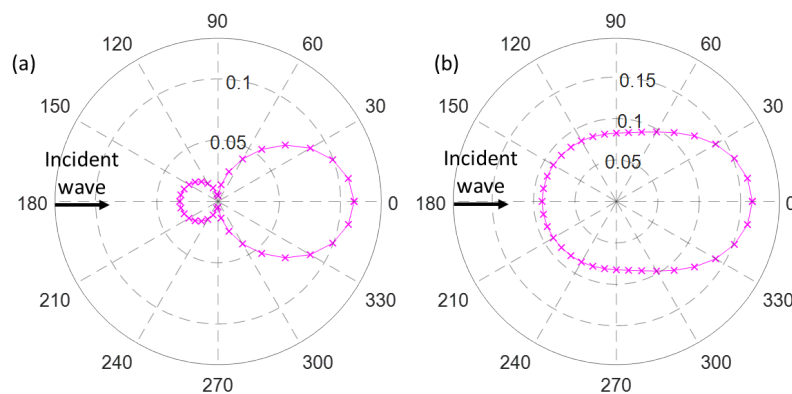
Fig. 11. SDPs for the one-side water-loaded plate with a 6mm diameter circular blind hole with a depth of (a) 1.0 mm and (b) 1.5mm

6. Advantages of quasi-Scholte waves for damage detection

In the foregoing studies, it has been demonstrated that it is feasible to utilize guided waves for detecting damages in submerged structural components. One of the biggest challenges in terms of practical applications is that guided waves have multimodal features. For example, within the frequency-thickness range up to 1MHz-mm, there are only quasi-Scholte waves, leaky A_0 waves, and leaky S_0 waves existing simultaneously on the one-side water-loaded steel plate. Other higher-order wave modes will appear if the excitation frequency is higher [9]. When the

measured signals contain multiple guided wave modes, it is very difficult to extract the damage-related wave signals that convey the information about the damage. Therefore, the use of guided waves at low excitation frequencies for damage detection is much more preferable since the measured signal has limited guided wave modes, which does not require sophisticated signal processing techniques.

Among these aforementioned three wave modes at the low-frequency band, leaky A_0 waves and leaky S_0 waves continuously radiate energy into the surrounding medium. Leaky A_0 waves have mostly out-of-plane displacements and decay rapidly due to the significant energy leakage into water. While leaky S_0 waves have a small attenuation because it is dominated by the in-plane motions. But leaky S_0 waves are relatively insensitive to the shallow surface corrosion since most of it is wave energy is confined to the mid-plane region of the plate [13, 40]. Unlike the leaky A_0 mode and the leaky S_0 modes, the quasi-Scholte mode is an interface wave mode whose energy is confined to the water-plate interface instead and does not significantly radiate into the water. This behavior enables the quasi-Scholte wave mode to travel over long distances with very low attenuation. In addition, the quasi-Scholte wave mode has a much smaller wavelength than leaky A_0 waves and leaky S_0 waves, which means that quasi-Scholte waves are more sensitive to small-scale damage at the same excitation frequency. Section 3 and Section 4 have numerically and experimentally demonstrated that at low frequencies, quasi-Scholte waves dominate over other wave modes when a circular piezoceramic transducer is installed on the water-free surface of the one-side water-immersed plate to excite guided waves. This phenomenon indicates that damage in the submerged structures can be potentially detected and evaluated based on a single wave mode. This significantly simplifies the practical implementations. In recognition of the above observations, it can be finally concluded that the quasi-Scholte wave mode is promising for damage detection in submerged structures. However, it should be noted that only the quasi-Scholte waves at low frequency-thickness range (in the dispersive region) could be applicable for detecting damage in the submerged structures. Because at higher frequency range where the quasi-Scholte mode is non-dispersive, the signal of quasi-Scholte waves cannot be detected from the plate surface since the displacements in the plate are negligible compared to the displacements in the water (see, Fig.3).

7. Conclusion

This paper has presented a study on guided wave propagation in a steel plate with one side immersed in water for SHM application on water-filled tanks and pipes, in particular, the focus has been directed on the interface wave mode, quasi-Scholte waves, and its scattering characteristics at circular blind holes. This interface wave mode at low frequencies has low attenuation and most of the excitation energy is conserved in the structures during the propagation. A 3D FE model has been developed to simulate the guided wave propagation in a steel plate exposed to water on one side. It has been confirmed that the signal measured from the water-free surface of the one-side water-immersed plate, which is excited by a circular piezoceramic transducer, is dominated by quasi-Scholte waves. The accuracy of the simulation results has been verified by comparing the phase velocities with the theoretical dispersion curves as well as the experimental measurements. The numerical simulations of wave scattering of the quasi-Scholte mode at a circular blind hole have been compared with the experimental measurements. A good agreement has been observed between the FE simulations and experimental measurements. It has been concluded the 3D FE model is able to accurately simulate quasi-Scholte wave propagation and its scattering characteristics for non-regular geometries.

Further numerical studies have demonstrated that the scattering directivity patterns (SDPs) depends on both the diameter and the depth of the circular blind hole. At a given depth of the damage, the amplitudes of the backward scattered waves are comparable to the forward scattering amplitudes for small values of R_{DW}. For larger R_{DW}, the forward scattering amplitudes increase quickly with slight variation while the backward scattering magnitudes fluctuate following a sinusoidal pattern with the overall trend being a slow increase. In general, the forward scattered waves are more suitable to be used for identifying the size of the damage since they have larger amplitudes and follow a relatively simple scattering pattern. For the local damage of the same diameter, the forward and backward scattering amplitudes increase with the depth of the damage. The backward scattering amplitudes increase faster than the forward scattered waves. Also, for the directions perpendicular to the incident wave, the scattering amplitudes are weak for damage whose depth is less than half of the plate thickness, but significantly increase for deeper damage.

Finally, this study has provided a comprehensive investigation of the scattering phenomena due to low-frequency quasi-Scholte waves interaction with a circular blind hole. The findings of this study can be used to provide a guide on selecting appropriate excitation

frequencies, guided wave modes, and transducer locations, and hence, it will help to improve the performance of in-situ damage detection techniques for structures exposed to the corrosive environment.

Acknowledgment

References

1. Yeung, C. and Ng, C.T., Time-domain spectral finite element method for analysis of torsional guided waves scattering and mode conversion by cracks in pipes. Mechanical Systems and Signal Processing, 2019. 128: p. 305-317.

2. Zhang, Z., Zhan, C., Shankar, K., Morozov, E.V., Singh, H.K., and Ray, T., Sensitivity analysis of inverse algorithms for damage detection in composites. Composite Structures, 2017. 176: p. 844-859.

3. Zheng, T., Luo, W., Hou, R., Lu, Z., and Cui, J., A novel experience-based learning algorithm for structural damage identification: simulation and experimental verification. Engineering Optimization, 2019: p. 1-24.

4. Mitra, M. and Gopalakrishnan, S., Guided wave-based structural health monitoring: A review. Smart Materials and Structures, 2016. 25(5): p. 053001.

5. Yu, X., Fan, Z., Castaings, M., and Biateau, C., Feature guided wave inspection of bond line defects between a stiffener and a composite plate. NDT & E International, 2017. 89: p. 44-55.

6. Qi, H., Xiang, M., and Guo, J., Scattering of a shear horizontal wave by a circular cavity in a piezoelectric bi-material strip based on guided wave theory. Mathematics and Mechanics of Solids, 2020. 25(4): p. 968-985.

7. Chua, C.A., Cawley, P., and Nagy, P.B., Scattering of the Fundamental Shear Guided Wave From a Surface-Breaking Crack in Plate-Like Structures. IEEE Transactions on Ultrasonics, Ferroelectrics, and Frequency Control, 2019. 66(12): p. 1887-1897.

8. Pudipeddi, G.T., Ng, C.T., and Kotousov, A., Mode Conversion and Scattering of Lamb Waves at Delaminations in Composite Laminates. Journal of Aerospace Engineering, 2019. 32(5): p. 04019067.

9. Takiy, A.E., Kitano, C., Higuti, RT., Granja, S.C.G., Prado, V.T., Elvira, L., and Martinez-Graullera, O., Ultrasound imaging of immersed plates using high-order Lamb modes at their low attenuation frequency bands. Mechanical Systems and Signal Processing, 2017. 96: p. 321-332.

10. Na, W.B., and Kundu, T., Underwater pipeline inspection using guided waves. Journal of pressure vessel technology, 2002. 124(2): p. 196-200.

11. Chen, J., Su, Z., and Cheng, L., Identification of corrosion damage in submerged structures using fundamental anti-symmetric Lamb waves. Smart Materials and Structures, 2009. 19(1): p. 015004.

12. Pistone, E., Li, K., and Rizzo, P., Noncontact monitoring of immersed plates by means of laser-induced ultrasounds. Structural Health Monitoring, 2013. 12(5-6): p. 549-565.

13. Sharma, S. and Mukherjee, A., Damage detection in submerged plates using ultrasonic guided waves. Sadhana, 2014. 39(5): p. 1009-1034.

14. Cegla, F.B., Cawley, P., and Lowe, M.J.S., Material property measurement using the quasi-Scholte mode—A waveguide sensor. The Journal of the Acoustical Society of America, 2005. 117(3): p. 1098-1107.

15. Tian, Z. and Yu, L., Study on guided wave propagation in a water loaded plate with wavenumber analysis techniques. in AIP Conference Proceedings, vol. 1581, no. 1, pp. 365-372. American Institute of Physics, 2014.

16. Tian, Z. and Yu, L., Lamb wave structural health monitoring using frequency-wavenumber analysis. in AIP Conference Proceedings , vol. 1511, no. 1, pp. 302-309. American Institute of Physics, 2013.

17. Hayashi, T. and Fujishima, R., Defect Detection Using Quasi-Scholte Wave for Plate Loaded with Water on Single Surface. Materials Transactions, 2016: p. M2016204.

18. Jaya, P.K. and Joseph, L.R., Mode controlled guided wave tomography using annular array transducers for SHM of water loaded plate-like structures. Smart Materials and Structures, 2013. 22(12): p. 125021.

19. Ng, C.T., Mohseni, H., and Lam, H.F., Debonding detection in CFRP-retrofitted reinforced concrete structures using nonlinear Rayleigh wave. Mechanical Systems and Signal Processing, 2019. 125: p. 245-256.

20. Masserey, B. and Fromme, P., In-situ monitoring of fatigue crack growth using high frequency guided waves. NDT & E International, 2015. 71: p. 1-7.

21. Rose, J.L., Ultrasonic guided waves in solid media. 2014: Cambridge university press.

22. Rizzo, P., Han, J.G., and Ni, X.L., Structural health monitoring of immersed structures by means of guided ultrasonic waves. Journal of Intelligent Material Systems and Structures, 2010. 21(14): p. 1397-1407.

23. Hayashi, T. and Inoue, D., Guided wave propagation in metallic and resin plates loaded with water on single surface. in AIP Conference Proceedings, vol. 1706, no. 1, p. 030003. AIP Publishing LLC, 2016.

24. Hayashi, T. and Inoue, D., Calculation of leaky Lamb waves with a semi-analytical finite element method. Ultrasonics, 2014. 54(6): p. 1460-1469.

25. Guo, P., Deng, B., Lan, X., Zhang. K., Li, H., Tian, Z., and Xu, H., Water Level Sensing in a Steel Vessel Using A0 and Quasi-Scholte Waves. Journal of Sensors, 2017. 2596291.

26. Yu, L. and Tian, Z., Case study of guided wave propagation in a one-side water-immersed steel plate. Case Studies in Nondestructive Testing and Evaluation, 2015. 3: p. 1-8.

27. Pavlakovic, B. and Lowe, M., Disperse user manual: a system for generating dispersion curves. Copyright B Pavlakovic, M Lowe, 2003.

28. Aubert, V., Wunenburger, R., Valier-Brasier, T., Rabaud, D., Kleman, J.P., and Poulain, C., A simple acoustofluidic chip for microscale manipulation using evanescent Scholte waves. Lab on a Chip, 2016. 16(13): p. 2532-2539.

29. Abaqus, Abaqus 6.13 Analysis User's Guide. Dassault Systems, Providence, RI, 2013.

30. Yang, Y., Ng, C.T., and Kotousov, A., Second Harmonic Generation of Guided Wave at Crack-Induced Debonding in FRP-Strengthened Metallic Plates. International Journal of Structural Stability and Dynamics, 2019. 19(01): p. 1940006.

31. Aryan, P., Kotousov, P., Ng, C.T., and Cazzolato, B., A model-based method for damage detection with guided waves. Structural Control and Health Monitoring, 2017. 24(3): p. e1884.

32. Aryan, P., Kotousov, A., Ng, C.T., and Wildy, S., Reconstruction of baseline time-trace under changing environmental and operational conditions. Smart Materials and Structures, 2016. 25(3): p. 035018.

33. Alleyne, D.N., and Cawley, P., The interaction of Lamb waves with defects. IEEE transactions on ultrasonics, ferroelectrics, and frequency control, 1992. 39(3): p. 381-397.

34. Yang, Y., Ng, C.T., Mohabuth, M., and Kotousov, A., Finite element prediction of acoustoelastic effect associated with Lamb wave propagation in pre-stressed plates. Smart Materials and Structures, 2019. 28(9): p. 095007.

35. Rajagopal, P., Drozdz, M., Skelton, E.A, Lowe, M.J., and Craster, R.V., On the use of absorbing layers to simulate the propagation of elastic waves in unbounded isotropic media using commercially available finite element packages. NDT & E International, 2012. 51: p. 30-40.

36. Mohseni, H. and Ng, C.T., Rayleigh wave propagation and scattering characteristics at debondings in fibre-reinforced polymer-retrofitted concrete structures. Structural Health Monitoring, 2019. 18(1): p. 303-317.

37. Pettit, J.R., Walker, A., Cawley, P., and Lowe, M., A stiffness reduction method for efficient absorption of waves at boundaries for use in commercial finite element codes. Ultrasonics, 2014. 54(7): p. 1868-1879.

38. Mohseni, H. and Ng, C.T., Higher harmonic generation of Rayleigh wave at debondings in FRP-retrofitted concrete structures. Smart Materials and Structures, 2018. 27(10): p. 105038.

39. Xie, Q., Ni, C., and Shen, Z., Defects Detection and Localization in Underwater Plates Using Laser Laterally Generated Pure Non-Dispersive S0 Mode. Applied Sciences, 2019. 9(3): p. 459.

40. Sharma, S. and Mukherjee, A., Ultrasonic guided waves for monitoring corrosion in submerged plates. Structural Control and Health Monitoring, 2015. 22(1): p. 19-35.